Progress In Electromagnetics Research B, Vol. 59, 45–58, 2014

Rainfall Microstructural Analysis for Microwave Link Networks: Comparison at Equatorial and Subtropical Africa

Akintunde Alonge* **and Thomas Afullo**

Abstract—The quest to understand the variation of rainfall microstructures at subtropical and equatorial regions is vital to rain attenuation studies. In this study, point rainfall datasets obtained at Butare (2°36′S, 29°44′E) and Durban (29°52′S, 30°58′E), are compared at the reflectivity threshold of 38 dBZ. Joss-Walvogel (JW) distrometer measurements collected from these two locations represent physical rainfall data from equatorial and subtropical climates respectively. The reflectivity threshold enables the classification of rainfall datasets into stratiform and convective (S-C) precipitation regimes. These thresholds, R_{th}, at Durban and Butare are analysed based on three known rainfall microphysical parameters: rain rate, rainfall Drop Size Distribution (DSD) and radar reflectivity. The results from rain rate distributions at the both regions are similar for both stratiform and convective classes. However, the sampled DSDs indicate the dominance of larger rain droplets at Butare compared to observations at Durban, irrespective of the rain classes. In addition, it is found that the reflectivity distributions at both regions, under stratiform and convective conditions, are distinct in their probability profiles. The overall S-C analysis implied that the reflectivity and DSD profiles at both regions — result in significant variation of predicted specific attenuation — at microwave and millimeter band. In comparison with other global locations, it is affirmed that the S-C transition occurs globally at rain rates between 6 mm/h and 13 mm/h.

1. INTRODUCTION

Rainfall attenuation is a major source of concern to communication systems operating at 10 GHz and beyond [1, 2]. Bands in this category support a wide range of microwave and millimeter wave systems, which are useful to the future viability of wireless networks in the contemporary provisioning of broadband communication services. Hybrid networks supported by satellite and terrestrial microwave links require high-speed connection, and hence, higher frequency spectrum to deliver sophisticated low-end services to customers. However, wireless networks transmitting beyond 10 GHz are often limited by the effects of rainfall attenuation. The mechanism of rainfall attenuation is reliant on the scattering and absorption of transmitted signal energy by rainfall droplets. This mechanism is dependent on frequency, drop-shape and temperature [3, 4]. The amount of transmitted energy absorbed or scattered is dependent on the prevailing raindrop size and rainfall rate, both of which are often inhomogeneous in space and time, during rain events. Thus, for a rain event, it is very likely to experience different attenuation within a swept area, at the same rainfall rate due to the varying number of rain drops of different sizes [5].

The obstruction of the strongest signature of Fresnel ellipsoids by dense columns of rain droplets in a swept area can be estimated by quantifying reflectivity via the processing of electronic data from radar systems or alternative ground measurements. Ground or space-borne radar measurements both estimate reflectivity parameters with background information on rain DSD and droplet densities [6, 7].

Received 11 February 2014, Accepted 8 March 2014, Scheduled 18 March 2014

* Corresponding author: Akintunde Alonge (dtanthony740@gmail.com).

The authors are with the Discipline of Electrical, Electronics and Computer Engineering, University of KwaZulu-Natal, Durban, South Africa.

In the absence of radars, the rainfall distrometer or rain gauge networks can be deployed to provide alternative measurements of rain rate and droplet density. Better still, it can provide information related to rainfall indices such as Liquid Water Content (LWC), rain rate and radar reflectivity [8].

Generally, rainfall process during a rainfall event can be considered to have three-stage constituent regimes: stratiform, transitional and convective [9, 10]. Researchers have reported the existence of these regimes in relation to their prevailing cloud types leading to rain events. For instance, Houze [11] reported that stratiform precipitations ($\sim< 20$ mm/h) are usually associated with strong horizontal profile, with widespread and low rain rates over a large cell area. They are formed from nimbostratus clouds and appear as bright bands under radar [11]. Convective precipitations ($\sim> 20$ mm/h), on the other hand, are induced from cumulus and cumulonimbus cloud formations. They are reputed to have stronger and columnar vertical profiles with characteristically small rain cells (less than 4 km in diameter) [11, 12]. The transition portion, as observed in the studies of Kumar et al. [7], mostly exists as a buffer regime during intense rainfall, between stratiform and convective regimes or vice versa. Generally, the stratiform portion of a rain event is mainly responsible for drizzle and widespread rainfalls, while, the convective portion generates rainfall of showers and thunderstorms. Classifying of precipitation datasets assists in the understanding of cloud physics and rainfall retrieval process from measurements [11]. It is also important in the studies of radio links, particularly in the allocation of advection velocities for the estimation of rain cell areas [13]. There are different methods of classifying Stratiform and Convective (S-C) regimes from distrometer and radar measurements [14, 15]. Some of these methods include the Background-Exceeding Technique (BET) for ground measurements and Precipitation Radar (PR) algorithms for processing radar images. For simplicity, this study employs the reflectivity threshold of 38 dBZ for the S-C classification proposed by Gamache and Houze [16].

Rainfall attenuation is a subject of interest at locations of immense and intense rainfall events. More so, areas located at low and mid latitudes around the world have been of interest to radio engineers — as they have unstable levels of rain fade. In this study, rainfall data obtained from the RD-80 JW distrometer measurements at equatorial and subtropical sites are compared using the microphysics of rainfall rate, rainfall DSD and radar reflectivity. The measurements of rainfall events collected at the two sites, Durban, South Africa and Butare, Rwanda, are taken as a single data — and then processed accordingly to determine their S-C thresholds. These thresholds, as computed at the two sites, are then applied as theoretical boundaries to separate the rainfall measurements into stratiform and convective regimes. Furthermore, the specific attenuation due to rain at both sites are predicted via Mie scattering technique and duly compared. Finally, the 38 dBZ approach is applied to determine and compare S-C thresholds at other global sites, using the available radar and DSD information.

2. MEASUREMENT AND DATA PROCESSING

In the absence of conventional radar-derived data, the Joss-Waldvogel RD-80 distrometer was employed at the sites in Durban, South Africa and Butare, Rwanda for the measurement of rainfall microstructural parameters. The distrometer unit processes rainfall data at one minute interval into 20 categorised channels of diameters between 0.3 mm to 5.3 mm, with an accuracy of $\pm 5\%$ [17]. Rainfall rate, rainfall drop number and radar reflectivity are among the notable parameters measured by the distrometer. At Durban, the equipment was installed at the University of KwaZulu-Natal (UKZN), Howard College Campus, Durban, from January 2009 to December 2010. At the other site, the equipment was installed at the National University of Rwanda (NUR), Butare, with a shorter period — between March 2012 and December 2012. For data processing, rainfall measurements with aggregate number of drops less than 10 were discarded; this is to minimize the underlying effects of dead time errors. Additionally, only rainfall samples exceeding 1 mm/h were considered, so that at Durban and Butare, a total of 8073 and 3659 useful rainy samples were processed, respectively. The maximum rainfall rate recorded at Durban and Butare is 117.15 mm/h and 78.52 mm/h respectively. A summary of all the distrometer measurements and other informative details are presented in Table 1.

At this point, understanding the unique geographic and climatic conditions at the two measurement locations is pertinent to this study. Butare, is located at a South-Western, low-latitude coordinates (close to the Equator) of $2°36'$S and $29°44'$E of the country of South-Western Rwanda. The equatorial conditions at this location induce the prevalence of super-tropical climate resulting in severe

Table 1. Site locations and measurement specifics.

Location	Total Rainfall (mm)	Lat °S	Long °E	No. of Rainy Events	Samples (minutes)		Climatic Features
					Collected	Filtered	
DURBAN	703.34	29°52′	30°58′	242	86470	8073	Subtropical
BUTARE	561.43	2°36′	29°44′	74	19973	3659	Equatorial

thunderstorms and strongly convective rains. Highland features are prominent with terrain elevation of 1.7 km above sea level, hence, mountainous [18]. Unlike the super-tropical climatic features present at Butare, Durban is located at mid-latitude coordinates of 29°52′S and 30°58′E, with an underlying subtropical climate along the East coast of South Africa. The rainfall pattern appears as a combination of temperate and tropical patterns — characterized by a combination of stratiforms and few cases of strong thunderstorms. In addition, Durban possesses a natural coastline of 28 m height above sea level, with the annual climate modulated by the easterly Indian and Atlantic Ocean currents. Apart from these features, these locations also have different structures of seasonal cycles with Butare experiencing wet and dry seasons occurring twice in its annual cycle. On the other hand, Durban experiences a four-season annual cycle comprising of summer, autumn, winter and spring.

3. RADAR RF DATA CLASSIFICATION FOR THE STRATIFORM-CONVECTIVE BOUNDS

The data from the JW distrometer consists of rain drop number statistics and derived rainfall rate. To classify the measurements from the two sites into S-C samples, their radar reflectivity indices are computed using the appropriate algorithm. Therefore, the Radar Reflectivity Factor (RRF) algorithm related to the sixth moment of rainfall DSD is computed. This is given by:

$$Z = \sum_{i=1}^{20} N\left(D_i\right) D_i^6 \Delta D_i \ \left[\mathrm{mm^6 m^{-3}}\right], \tag{1}$$

and, the reflectivity in dBZ given as:

$$Z = 10\log_{10}\left(Z\right) \ [\mathrm{dBZ}] \tag{2}$$

where $N(D_i)$ is the rainfall DSD of the ith channel computed from the distrometer [5]:

$$N\left(D_i\right) = \frac{C_i}{A \times T \times v\left(D_i\right) \times D_i} \ \left[\mathrm{mm^{-1} m^{-3}}\right] \tag{3}$$

where C_i is the number of drop available at the ith channel, A the sampling area of the distrometer cone set as $0.005\,\mathrm{m}^2$, T the sampling interval given as 60 seconds, $v(D_i)$ the terminal velocity of the ith channel, and ΔD_i the diameter interval of the ith channel.

The computed radar RF (Z), as explained by earlier authors, can be represented as a simple power-law function dependent on rainfall rate (R) [19–21]. This expression, also known as Z-R relationship, proposed by Marshall and Palmer [19] is given as:

$$Z = AR^b \ [\mathrm{mm^6 m^{-3}}] \tag{4}$$

where A and b from numerous studies are coefficients dependent on geographical and climatic factors. The standard Z-R expression given in their study was computed as $A = 200$ and $b = 1.6$ from the exponential DSD for European climate. Battan [20], in addition, also produced Z-R results for 69 locations around the world.

By combining (1)–(3), the coefficients A and b for continuous rainfall at Durban and Butare are obtained by regression technique. In Table 2, we present results of the monthly rainfall parameters at Durban and Butare. At Durban, peak reflectivities vary over the months annually with the highest value of 55.15 dBZ observed in the month of April. This coincides with the recorded peak rain rate of 117.15 mm/h. The b coefficients of the Z-R parameter are seen to be fairly constant (~ 1.55) from

Table 2. An overview of monthly rain statistics from measurements at Durban and Butare.

Location	Month	Duration (min)	Acc. (mm)	Peak Rain Rate (mm/h)	Peak Reflect. (dBZ)	Z-R function
DURBAN	JAN	1396	88.25	48.93	47.22	$126R^{1.55}$
	FEB	974	56.76	49.38	46.46	$170R^{1.56}$
	MAR	522	42.13	66.25	47.34	$104R^{1.55}$
	APR	630	54.40	117.15	55.15	$147R^{1.58}$
	MAY	651	44.47	76.43	51.54	$602R^{1.24}$
	JUNE	231	3.59	38.61	54.99	$197R^{2.05}$
	JULY	34	3.08	23.36	43.61	$342R^{1.60}$
	AUG	621	23.04	12.59	50.17	$333R^{1.67}$
	SEP	388	16.46	18.57	40.59	$88R^{1.66}$
	OCT	216	15.61	20.37	41.57	$86R^{1.62}$
	NOV	541	39.61	57.67	47.99	$83R^{1.65}$
	DEC	1671	109.13	47.83	56.96	$124R^{1.54}$
BUTARE	MAR	215	26.41	68.33	54.42	$270R^{1.59}$
	APR	1119	90.03	78.52	52.24	$267R^{1.46}$
	MAY	174	34.39	73.99	51.46	$244R^{1.42}$
	JUNE	609	72.13	56.71	50.88	$208R^{1.50}$
	JULY	-NR-	X	X	X	X
	AUG	271	25.79	60.94	51.78	$296R^{1.37}$
	SEP	279	23.60	35.96	47.39	$276R^{1.57}$
	OCT	662	51.70	71.59	51.92	$304R^{1.39}$
	NOV	330	36.2	46.84	50.71	$245R^{1.48}$

December to May which coincides with the period of summer and autumn. Elsewhere, the values are also seen to be close between September and November (~ 1.65). For the entire year, the averaged peak reflectivity is 48.63 dBZ. At Butare, the monthly peak reflectivity also varies over the year. The highest value is observed in March at 54.42 dBZ and fails to correspond to the peak rainfall rate. The peak reflectivity is also seen to decrease from March to June, with a dry spell in July. Thereafter, the reflectivity remains fairly constant. For the overall datasets in both cases, the overall Z-R coefficients are obtained with Durban ($A = 157.76$, $b = 1.52$) and Butare ($A = 265.6$, $b = 1.45$). The coefficients at Butare are slightly close to those obtained in the studies of continental and equatorial Africa by Ochou et al. [22], and, Sauvageot and Lacaux [23]. At Durban, the coefficients are observed to appear closer to the earlier results of [19] with lower value of A.

The determination of S-C thresholds for the datasets at the two sites is computed using the 38 dBZ threshold proposed by Gamache and Houze [16]. Equations (2) and (4) are modified so that the rainfall rate transition threshold, R_{th}, at 38 dBZ is determined by:

$$\log(R_{th}) = \frac{3.8 - \log(A)}{b} \tag{5}$$

where R_{th} is the rainfall rate at the S-C threshold in mm/h.

By computation, these thresholds (R_{th}) at Durban and Butare are found to be 11.34 mm/h and 8.84 mm/h respectively from their Z-R relationships. This shows that rainfall typically begins an 'early' transition into convective rainfall at Butare with about 2.5 mm/h lag behind Durban. On obtaining these thresholds, the filtered data at both locations are then reclassified into stratiform and convective rainfall regimes as seen in Figs. 1(a)–(d). A summary of the classified data samples for each regime at the sites is presented in Table 3. As seen in this table, stratiform precipitations account for about 95% and 85% of rainfall measurements at Durban and Butare respectively. Thus, about 5% and 15% of

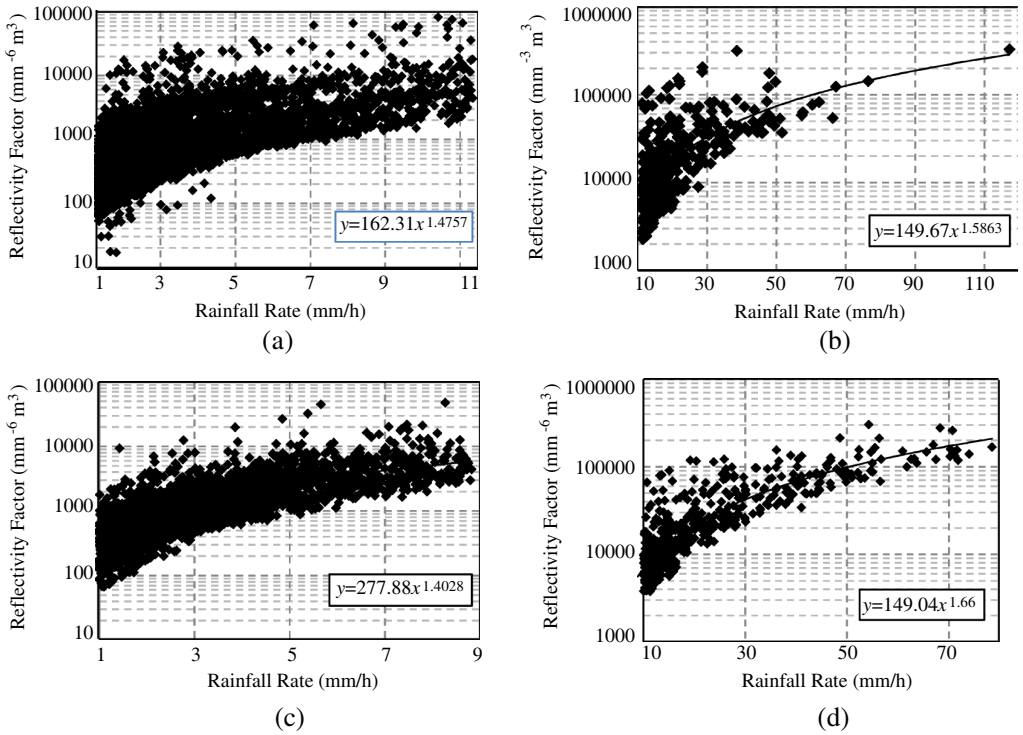

Figure 1. The continuous plots of radar reflectivity versus rainfall rate observed at the sites: (a) Durban — Stratiform ($R < 11.34$ mm/h), (b) Durban — Convective ($R > 11.34$ mm/h), (c) Butare — Stratiform ($R < 8.84$ mm/h), (d) Butare — Convective ($R > 8.84$ mm/h).

Table 3. Data samples of stratiform and convective rains for measurements at Butare and Durban.

LOCATION	STRATIFORM		CONVECTIVE	
	Samples	Z-R Fit	Samples	Z-R Fit
DURBAN	7667	$162.31R^{1.48}$	406	$149.67R^{1.59}$
BUTARE	3093	$277.88R^{1.40}$	566	$149.04R^{1.66}$

the overall classified data at both sites are convective samples. Again, the predominance of stratiform precipitation at the two sites is consistent with observations at mid-latitude areas, especially tropical regions [6, 24, 25].

By fitting the reflectivity samples at both sites for stratiform and convective regimes, it is found that A coefficients of the Z-R function for former regime is higher than that of the latter regime (see Table 3). Conversely, b coefficients for convective regime are higher than those observed for stratiform regime. At Butare, A coefficients for stratiform are higher than those observed at Durban. On the other hand, b convective regime than seen at Butare. A close similarity in the reflectivity coefficients is also observed under the convective regime with Durban ($A \sim 150$, $b \sim 1.59$), and Butare ($A \sim 149$, $b \sim 1.66$). This discovery signifies proximate rainfall structures at both sites for convective precipitation.

4. STATISTICAL COMPARISON OF RAIN MICROSTRUCTURAL PARAMETERSAT S-C PRECIPITATION BOUNDS

The variation of rainfall characteristics at equatorial and subtropical areas depends on the dynamics of their microphysics. Therefore, understanding the characteristics of rainfall microphysics under stratiform and convective regimes at both sites, is of utmost importance. To achieve this, the already classified datasets are examined statistically under three microphysical parameters namely: rainfall rate, rainfall DSD and radar reflectivity.

4.1. Comparison of Rainfall Rate Distributions at S-C Precipitation Bounds

The Complementary Cumulative Distribution Function (CCDF) of the rainfall rate datasets, for both stratiform and convective regimes, are generated as shown in Figs. 2(a) and 2(b). The maximum bound of the stratiform regime at both locations equals to the threshold obtained from (5). For the convective regime, the maximum bounds are 120 mm/h and 80 mm/h respectively at Durban and Butare respectively.

From Fig. 2(a), it is observed that the compared CCDF at Butare slightly exceeds that of Durban for stratiform regimes for the period of comparison. However, the CCDFs intercept at 6.3 mm/h and diverge due to the influence of the gradual breakaway as 38 dBZ thresholds are approached. From Fig. 2(b), the CCDF at Durban is seen to exceed that of Butare — for rain rates up to 20 mm/h for the convective regime. However, beyond this rain rate, Butare is seen to increasingly have higher exceedence values of CCDF than Durban until they intercept at around 74 mm/h; and thereafter diverges. Based on the observations from the CCDF comparisons under convective conditions, it is intuitive to note that Butare experiences higher exceedences than Durban beyond 20 mm/h, until both sites approach their breakpoints at about 1% of rain exceedence. This is the first indication of the presence of heavy thunderstorms at Butare compared to Durban. Due to the higher maximum rainfall rate recorded at Durban, rain rates beyond 0.1% of the exceeded time are higher under stratiform regime. Table 4 summarizes the rain distribution statistics at both sites exceeded at 0.1%, 0.01%, and 0.001% of the time. Evidently, these percentages are higher at Durban for both considered regimes as seen from the results.

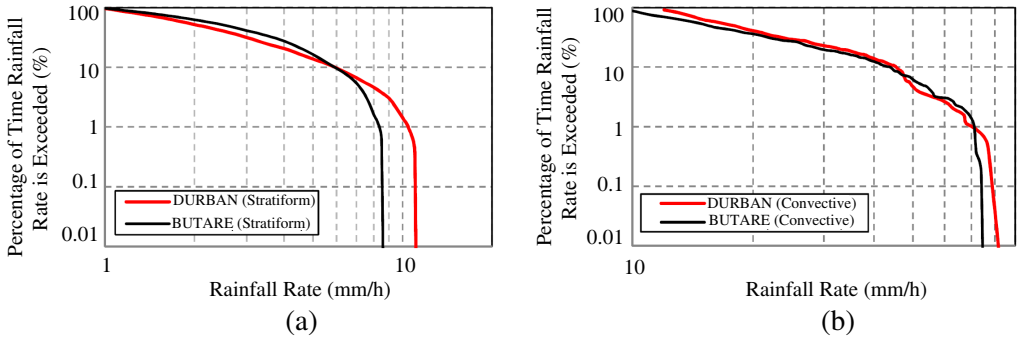

Figure 2. Rainfall rate distribution observed at Durban and Butare: (a) stratiform, (b) convective.

Table 4. Comparison of the S-C exceedence values from the rain rate CCDFs at Durban and Butare.

Time Percent (%)	STRATIFORM		CONVECTIVE	
	DBN	BTR	DBN	BTR
0.1	11.01	8.55	79.2	72.2
0.01	11.07	8.6	82.3	74.5
0.001	11.28	8.62	85.8	79

4.2. Comparison of Rainfall DSDs at S-CP Recipitation Bounds

The rainfall DSDs at the two sites based on stratiform-convective classes are compared by applying a known statistical distribution model. The preferred model selected for this study is the three-parameter lognormal distribution with three unknown variables. The lognormal model has been proposed in several research as the foremost model useful for rainfall DSD estimation at tropical and subtropical locations from measurements [1, 4]. The lognormal distribution for rain droplets is given as:

$$N(D_i) = \frac{N_T}{D_i \sigma \sqrt{2\pi}} \exp\left[-0.5\left(\frac{\ln(D_i) - \mu}{\sigma}\right)^2\right] \quad \text{for } N_T > 0;\ -\infty < \mu < +\infty;\quad \sigma > 0 \tag{6}$$

where N_T, μ and σ are the unknown variables with the diameter D_i as the only input obtained from measurement.

Using the Method of Moments (MoM) for parameter estimation, the variables corresponding to each rainfall regime at these locations are computed [26]. The 3rd, 4th and 6th moments of the measured rain dropsize data are used to obtain the three unknown lognormal parameters, based on their rainfall relationships [26]. The derived results obtained are given as regression functions dependent on the rainfall rate, R. Table 5 gives a summary of the functions representing the solved parameters obtained for each regime based on the lognormal parameters. The plots for the lognormal DSD model computed at different rainfall rates across the two investigated regimes are shown in Figs. 3(a)–(d). The rainfall rates investigated are at 5 mm/h, 15 mm/h, 40 mm/h and 80 mm/h.

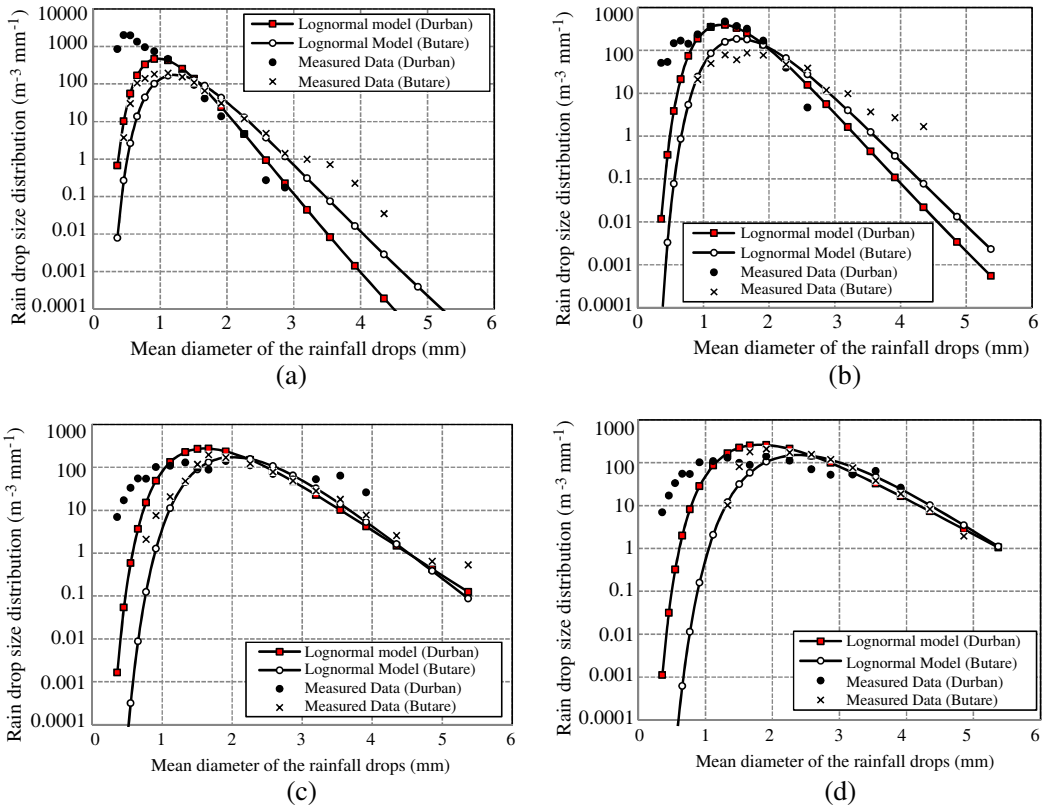

Figure 3. Rainfall DSD variation at Durban and Butare using the S-C bounds at different rain rates: (a) 5 mm/h, (b) 15 mm/h, (c) 40 mm/h, (d) 80 mm/h.

Table 5. Parameters of the lognormal distribution parameters for stratiform and convective rains.

BOUNDS	**PARAMETERS**	**DURBAN**	**BUTARE**
STRATIFORM BOUND	N_T	$300R^{0.0614}$	$101.72R^{0.2463}$
	μ	$-0.3441 + 0.2462\ \mathrm{Ln}(R)$	$-0.0776 + 0.2133\ \mathrm{Ln}(R)$
	σ^2	$0.075 + 0.0005\ \mathrm{Ln}(R)$	$0.0818\text{-}0.005\ \mathrm{Ln}(R)$
CONVECTIVE BOUND	**PARAMETERS**	**DURBAN**	**BUTARE**
	N_T	$170.39R^{0.2011}$	$161.3R^{0.0805}$
	μ	$-0.1295 + 0.1903\ \mathrm{Ln}(R)$	$-0.1587 + 0.2498\ \mathrm{Ln}(R)$
	σ^2	$0.0275 + 0.018\ \mathrm{Ln}(R)$	$0.0439 + 0.0053\ \mathrm{Ln}(R)$

Firstly, it is observed that the distribution of small droplets in Butare decreases rapidly as the rainfall rates increases, while transiting from stratiform to convective regimes. In fact, this anomaly is much more severe for the rain droplets under convective regimes with small rain drop sizes (with diameter less than 0.913 mm) having DSDs less than one and tending to zero. In contrast, Durban is seen to experience higher scales of DSDs for both stratiform and convective regimes. Interestingly, it is also observed that larger raindrop sizes have higher statistical representation at Butare for stratiform regime, than seen in Durban (please see Figs. 3(a) and 3(b)). However, for convective regime, the DSDs of large droplets are similar at both Durban and Butare ($\sim >$ 2.5 mm). This suggests that the structural distribution profile of large rain droplets at Butare and Durban are slightly similar under convective conditions. However, the near-absence of smaller droplets ($\sim <$ 2.5 mm) at the Rwandan site (please see Figs. 3(c) and 3(d)) under convective conditions, may be linked to its equatorial characteristics and its unique height above the sea level ($\sim$ 1.7 km). From research, it has been documented that areas around tropical regions have lower occurrence probabilities of smaller rain droplets, and hence, reduced population especially at high rainfall rates i.e., convective conditions [23, 27]. Additionally, the intense and 'super-tropical' structure of rainfalls at Butare — as with most locations around the equator — validates these observations. It might suffice to add that the integrity of large droplets produced from rain clouds will be much higher at this location. This is partly due to the near-passive nature of droplet disintegration mechanisms like rain height and wind effects during rainfall. The implication of this phenomenon will ultimately affect the contributions of rain droplets in wave scattering and absorption mechanism responsible for rain attenuation as will be explained later.

4.3. Comparison of Radar Reflectivity Distribution for S-C Rain Precipitation Bounds

The radar reflectivity distributions for stratiform and convective regimes obtained at Durban and Butare are shown in Figs. 4(a) and 4(b). It should be noted that applying the S-C rain rate threshold to the two-regime datasets result in 'smearing' of reflectivity values below and above the 38 dBZ threshold for stratiform and convective regimes as seen in Figs. 4(a) and (b). The 'smearing' is attributed to the randomness of the rainfall DSD generation process during rain events. Therefore, it is possible to have rainfall rate samples with values above 38 dBZ under stratiform conditions, and then below 38 dBZ under convective conditions.

In Fig. 4(a), the stratiform distributions at the two locations are seen as having similar shape profiles, albeit with different statistical mean (μ_z) and standard deviation (σ_z). While the radar reflectivity distribution at Durban is seen as having higher probabilities of reflectivities less than 28 dBZ, it is converse at Butare. This variation, we know is also related to the rainfall DSD — which translates to variation in the appearance of rain drop sizes. Firstly, it should be noted that under stratiform DSDs, the visible presence of small rain droplets is responsible for the lower values of radar reflectivities less

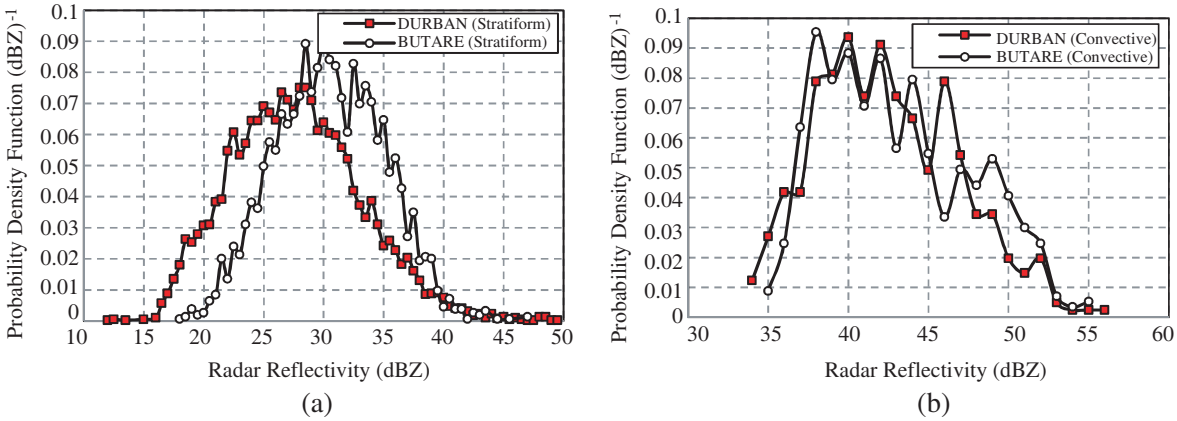

Figure 4. The radar reflectivity distributions for stratiform and convective rainfall bounds: (a) Durban, (b) Butare.

than 18 dBZ, at Durban. In the case of Butare, reflectivity samples greater than 28 dBZ have higher occurrence probability than seen at Durban. This again is due to the obvious presence of large droplets for the stratiform DSD profile as earlier explained (see Section 4.2). For the convective conditions as seen in Fig. 4(b), the shape profiles of the reflectivity distribution at both locations are strikingly similar. The shape profiles of the radar reflectivity probabilities at both locations are evidently normally distributed and can be statistically described by a Gaussian distribution function given by:

$$p\left(Z\right) = \frac{1}{\sigma_z\sqrt{2\pi}} \exp\left[-\frac{1}{2}\left(\frac{Z-\mu_z}{\sigma_z}\right)^2\right] \ [\text{dBZ}]^{-1} \tag{7}$$

The parameters, μ_z and σ_z, from (7) are obtained for the two sites by applying the method of maximum likelihood parameter estimation technique.

The radar reflectivity data are further analysed based on the stratiform and convective regimes. For stratiform class, the set of parameters estimated at Durban ($\mu_z = 27.42$, $\sigma_z = 5.42$) and Butare ($\mu_z = 30.24$, $\sigma_z = 4.5$) are with Root-Mean Square (RMS) errors of 0.31% and 0.62% respectively. Likewise, the parameters for the convective classes are found accordingly with Durban ($\mu_z = 41.94$, $\sigma_z = 4.41$) and Butare ($\mu_z = 42.54$, $\sigma_z = 4.6$) having corresponding RMS values of 1.76% and 1.06% respectively.

Again, the close values of computed parameters under convective conditions at both locations, indicates a similarity in the rainfall structures for showers and thunderstorms. To confirm this from the earlier results in Table 3, the A coefficients for convective Z-R relationship at Butare (~ 149.04) and Durban (~ 149.67) are also close. Even at that, their b coefficients are closer with Butare (~ 1.66) and Durban (~ 1.59) with the former having a higher value. This pattern suggests a sort of similarity in the convective patterns at both locations, with the only noticeable difference being the scale of their Z-R functions. However, these characteristics may not translate into similar specific attenuation index as will be seen later. This is true because scattering of transmitted signals (forward scattering) required for attenuation is much more related to the transmission frequency and particle size.

4.4. Implications of Microphysical Variations on Rain Attenuation

Network engineers are mainly concerned with the performance of the link as telemetry is varied. Of particular interest is the extent of rainfall effects on link performances, during periods of fluctuating Received Signal Level (RSL). The specific attenuation is an indication of amount of the projected power losses due to rainfall (or rain fade) per kilometer. For simplification of computing results from rainfall DSD functions, the Mie scattering approach is used to compute these results. The specific attenuation can be computed using the equation given in [1] as:

$$A_S = 4.343 \times 10^{-3} \sum_{i=1}^{20} N\left(D_i\right) Q_{ext}\left(D_i\right) \Delta D_i \ [\text{dB/km}] \tag{8}$$

where $N(D_i)$ is the rain DSD, $Q_{ext}(D_i)$ is the extinction cross section in mm^2 and ΔD_i is the diameter interval.

The extinction cross section is simplified by the Mie scattering expression given as:

$$Q_{ext}\left(R\right) = \frac{4\pi}{k^2}\text{Re}\left\{S(0)\right\} \approx \ k_{ext}\left(R\right)^{\varsigma_{ext}} \ \left[\text{mm}^2\right] \tag{9}$$

where R is the radius of the rain droplets in mm, while, k_{ext} and ς_{ext} are the Mie coefficients obtained from elaborate computations of spherical Bessel functions. The computations for Durban at 20°C are undertaken at different water frequencies (up to 1 THz) using the single and double Debye method [28] with Mie parameters. At Butare, the same Mie computation procedure for Durban is applied with an assumed temperature of 20°C. At high rainfall rates, rain droplet spectra mainly appear as oblate-spheroid and spheroidal in shape. Thus, specific attenuation values predicted from Mie coefficients are limited in accuracy, especially for rain droplets at high rain rates.

By applying the results from Table 5, the specific attenuation for stratiform and convective rain regimes at both Durban and Rwanda are computed. The lognormal DSDs from both sites, generated

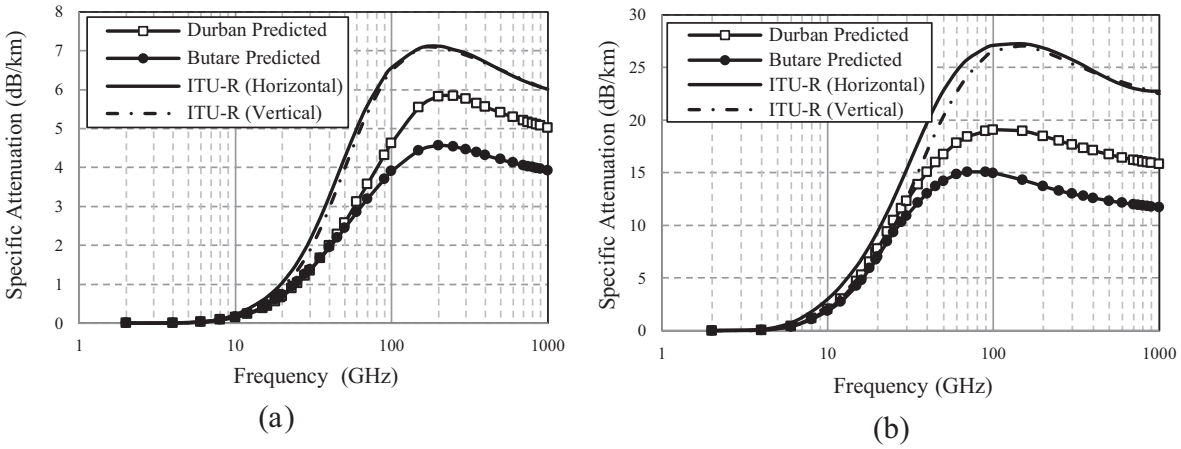

Figure 5. Specific attenuation at Durban and Butare computed with Mie technique at 20°C compared with ITU-R P.838-3 at (a) $R = 10$ mm/h, (b) $R = 80$ mm/h.

Table 6. Specific attenuation predicted from the lognormal distribution at Butare and Durban.

FREQUENCY (GHz)	DURBAN			BUTARE		
	RAIN RATE (mm/h)			RAIN RATE (mm/h)		
	10	25	80	10	25	80
4	0.01	0.02	0.07	0.01	0.02	0.07
8	0.08	0.29	1.18	0.09	0.29	1.09
10	0.15	0.51	2.05	0.16	0.51	1.88
15	0.38	1.21	4.68	0.41	1.21	4.26
20	0.69	2.10	7.76	0.73	2.09	7.02
25	1.03	2.98	10.46	1.07	2.93	9.37
30	1.35	3.69	12.33	1.37	3.61	10.91
40	1.98	4.94	15.05	1.94	4.72	13.04
45	2.29	5.46	15.99	2.20	5.17	13.71
50	2.58	5.92	16.76	2.44	5.57	14.23
60	3.11	6.69	17.81	2.85	6.18	14.83
90	4.32	8.09	18.94	3.70	7.17	15.06
100	4.62	8.40	19.07	3.90	7.36	14.98
200	5.83	9.22	18.47	4.56	7.69	13.70
300	5.75	8.95	17.65	4.46	7.41	12.99
400	5.55	8.66	17.10	4.31	7.18	12.60

from Eq. (6), are applied to generate their specific attenuations. As seen from the plots in Figs. 5(a) and (b), the specific attenuation at Butare start diverging from the Durban results at about 40 GHz.

The target rainfall rates of 10 mm/h, 25 mm/h and 80 mm/h are also investigated, over 4 GHz to 100 GHz transmission frequencies, as seen in Table 6. From Table 6, the predicted specific attenuation at Butare starts to decline at 40 GHz for a rain rate of 10 mm/h. At 25 mm/h, the decline is noticeable from 20 GHz; at 80 mm/h, the decline is noticed from 8 GHz. Broadly speaking, there is a rapid decline in the predicted specific attenuation as rainfall transit from stratiform to convective regimes at Butare. For obvious reasons, it seems that this decline of specific attenuation over high frequencies and high

rain rates is related to the relatively large population of larger rain droplets. We have earlier noted at this site, the dearth of smaller rain droplets, which ultimately plays an important role in the DSD and reflectivity profile. Recently, Adetan and Afullo [29] suggested a maximum diameter bound of ≤ 3.5 mm in the percentage of critical diameters responsible for specific attenuation at Butare. Furthermore, their studies reported a decline in the role(s) of these range of critical diameters in Butare compared to their observation at Durban. Their findings are consistent with the results in this study.

Therefore, the predicted specific attenuation is observed to be generally higher at South Africa than Rwanda, from about 30 GHz. However, both sites do have lower specific attenuation than the predicted specific attenuation values from ITU-R P.838-3 [30].

5. COMPARISON OF S-C RAIN RATE THRESHOLDS AT OTHER LOCATIONS

To examine the consistency of the computed results of S-C rain rate thresholds at Durban and Butare, a global comparison is considered. Therefore, Z-R results from other locations with different climato-meteorological scenarios are adequately compared. Some of the African locations are Ile-Ife, Nigeria [31], Benin Republic [32], Niger Republic [22], Senegal [24] and Congo [23]. The compared locations around the Asian region include Calcutta, India [33], Hassan and Ahmedabad at India [4] and Singapore [7]. The Oceania areas include Kapingamarangi, Micronesia [34] and Darwin, Australia [35]. Finally, some locations in the Americas include Canada [18] with other locations such as Florida, Marshall Islands and Oregon in the USA [36].

Parameters of proposed Z-R relationships from studies at some of these locations were applied to initially estimate R_{th}. Locations without available Z-R information were substituted with their equivalent rainfall DSD parameters, either from lognormal distribution or modified gamma distribution. Locations at which DSD functions are applied to obtain Z-R results include Ile-Ife, Calcutta, Hassan and Ahmedabad because of the aforementioned reason. The results containing Z-R parameters, R_{th} and $Z_{0.01}$ from the computations are presented in Table 7. The $R_{0.01}$ values are obtained directly from the ITU-R estimates from the global designation for different climatic zones in ITU-R P.837-6 [37]. The S-C rain rate transition threshold, R_{th}, tend to converge at 10 mm/h (or closer to 38 dBZ) as confirmed by previous studies [16, 24, 34]. However, we find that the transition rain rates at other locations have a deviation of about ± 3 mm/h from this convergent value, as influenced by their geographical and climatic factors. As seen from Table 7, the radar reflectivities at 0.01% of the exceeded rain rate, $Z_{0.01}$, computed at the compared global locations all seem to converge close to 50 dBZ — with a deviation of about ± 4 dBZ. From these comparisons, it is obvious that a positive correlation exists between the R_{th} and their corresponding $R_{0.01}$ as seen in Fig. 6. A power-law relationship is sufficient to describe the relationship between these two parameters as seen in Fig. 6. This relationship is given as:

$$R_{th} = 2.31 R_{0.01}^{0.34} \quad [\text{mm/h}] \tag{10}$$

From (10), it becomes obvious that the two parameters are positively correlated across the listed locations. This implies that areas with higher $R_{0.01}$ have a corresponding higher R_{th}, and vice-versa.

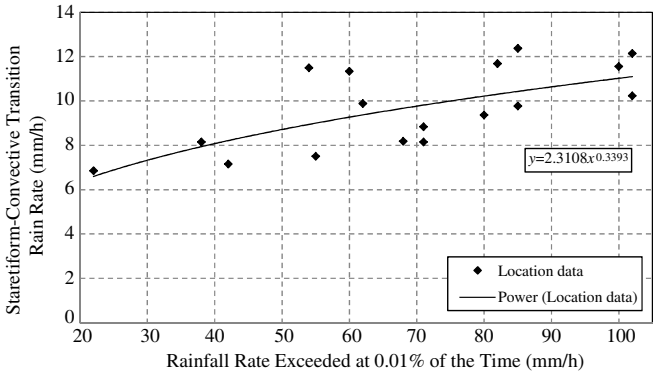

Figure 6. Comparison of $R_{0.01}$ and S-C thresholds for different locations around the world.

Table 7. Comparison of S-C thresholds at other global locations.

Zones	Sites	Location		Z-R Function		THRESHOLD (mm/h)	$R_{0.01}$ (mm/h)	$Z_{0.01}$ (dBZ)
		LAT	LONG	A	B			
AFRICA	S. AFRICA (Durban)	29.88°S	31.05°E	157.76	1.52	11.34	60	48.99
	RWANDA (Butare)	2.6°S	29.75°E	265.6	1.45	8.84	71	51.06
	NIGERIA (Ile-Ife)	7.47°N	4.567°E	396.24	1.32	8.18	68	50.12
	EQUITORIAL Congo	2.88°S	23.66°E	364	1.36	8.15	71	50.79
	NIGER (Niamey)	13.52°N	2.11°E	508	1.28	7.16	42	47.84
	SENEGAL (Dakar)	14.69°N	17.45°W	368	1.24	9.89	62	47.89
	BENIN	8.83°N	2.18°E	433	1.33	7.5	55	49.51
ASIA	INDIA (Calcutta)	22.57°N	88.37°E	106.68	1.67	11.56	100	53.62
	INDIA (Ahmedabad)	23.03°N	72.58°E	195.29	1.42	11.50	54	47.55
	INDIA (Hassan)	13.06°N	76.10°E	169.15	1.44	12.38	85	50.04
	SINGAPORE	1.30°N	103.80°E	285.83	1.33	10.24	102	51.28
AMERICAS	USA (Oregon)	44.00°N	120.50°W	295	1.59	6.86	22	46.04
	USA (Marshall Is.)	7.07°N	171.27°E	226	1.46	9.78	85	51.71
	USA (Florida)	28.10°N	81.60°W	322	1.33	9.37	80	50.39
	CANADA (Ottawa)	45.42°N	75.7°W	220	1.60	8.15	38	48.71
OCEANIA	MICRONESIA (Kapingamarangi)	1.07°N	154.78°E	315	1.20	12.15	102	49.09
	AUSTRALIA (Darwin)	12.45°S	130.83°E	170	1.47	11.69	82	50.44

6. CONCLUSION

The microphysical analysis undertaken in this study has revealed the variation in rainfall characteristics at sub-tropical and equatorial locations. The structures of the compared microphysical parameters, i.e., rain rate, rain DSD and reflectivity at Durban and Butare, varies with some similarities under stratiform regimes. However, these same parameters are similar at both locations under convective conditions. This implies that showers and thunderstorm rainfalls have the same characteristics at the compared locations. This characteristic does not suffice for predicted specific attenuation as there are substantial disparities in the DSD structures for rain droplets with sizes less than 2.5 mm. These disparities noticed at Butare result in a progressive decline of specific attenuation as carrier frequency is

scaled, irrespective of the rain rate. Indeed, this is purely based on geographic and climatic differences resulting in dearth of small rain droplets (≤ 3 mm). Based on this study, it is predicted that Butare is an ideal location for earth-space communication, especially for design frequencies above 40 GHz. This study has also found a correlation between the S-C transition rain rate (R_{th}) and $R_{0.01}$, where the former varies over a range of 6 mm/h $\leq R_{th} \leq$ 13 mm/h at the globally compared locations. However, the shorter measurement period at Butare is a limitation that could influence the overall cyclical rainfall patterns. Therefore, it is suggested that longer measurement period of rainfall statistics at both sites will greatly improve the knowledge of rainfall microphysics for radio link design. In conclusion, the results derived from this study will be beneficial to the knowledge of rain microphysics in radio and microwave engineering around the world.

ACKNOWLEDGMENT

The authors are gracious to Dr. Felix Akorli of the National University of Rwanda, Butare for the provision of disdrometer measurements applied in this study.

REFERENCES

1. Ajayi, G. O., S. Feng, S. M. Radicella, and B. M. Reddy, *Handbook on Radiopropagation Related to Satellite Communications in Tropical and Subtropical Countries*, 7–14, ICTP, Trieste, 1996.
2. Crane, R. K., *Electromagnetic Wave Propagation through Rain*, 1–40, John Wiley, New York, 1996.
3. Aydin, K. and S. E. A. Daisley, "Relationships between rainfall rate and 35-GHz attenuation and differential attenuation: Modeling the effects of raindrop size distribution, canting and oscillation," *IEEE Trans. Geosci. Remote Sens.*, Vol. 40, No. 11, 2343–2352, 2002.
4. Das, S., A. Maitra, and A. K. Shukla, "Rain attenuation modeling in the 10–100 GHz frequency using drop size distributions for different climatic zones in tropical India," *Progress In Electromagnetics Research B*, Vol. 25, 211–224, 2010.
5. Chen, K. S., C. Y. Chu, and Y. C. Tseng, "A semi-empirical model of rain attenuation at Ka-band in Northern Taiwan," *Progress In Electromagnetic Research M*, Vol. 16, 213–223, 2011.
6. Tenório, R. S., M. C. Da Silva Moraes, and B. H. Kwon, "Raindrop distribution in the eastern coast of northeastern brazil using disdrometer data," *Revista Brasileira de Meterologia*, Vol. 25, No. 4, 415–426, 2010.
7. Kumar, L. S., Y. H. Lee, J. X. Yeo, and J. T. Ong, "Tropical rain classification and estimation of rain from *Z-R* (Reflectivity-Rain Rate) relationships," *Progress In Electromagnetic Research B*, Vol. 32, 107–127, 2011.
8. Bartholomew, M. J., *Disdrometer and Tipping Bucket Raingauge Handbook*, DOE/SC-ARM/TR-079, ARM Climate Research Facility, 2009.
9. Tokay, A., D. A. Short, C. R. Williams, W. L. Ecklund, and K. S. Gage, "Tropical rainfall associated with convective and stratiform clouds: Intercomparison of disdrometer and profiler measurements," *J. Appl. Metor.*, Vol. 38, No. 3, 302–320, 1999.
10. Wilson, C. L. and J. Tan, "The characteristics of rainfall and melting layer in Singapore: Experimental results from radar and ground instruments," *11th International Conference on Antennas and Propagation*, Vol. 480, 852–856, 2001.
11. Houze, R. A., "Stratiform precipitation in regions of convection: A meteorological Paradox?," *Bulletin of the American Meteorological Society*, Vol. 78, No. 10, 1997.
12. Anagnostou, E. N., "A convective/stratiform precipitation classification algorithm for volume scanning weather radar observations," *Meteorol. Appl.*, Vol. 11, 291–300, 2004.
13. Begum, S., C. Nagaraja, and I. Otung, "Analysis of rain cell size distribution for application in site diversity," *First European Conference on Antennas and Propag. (EuCAP 2006)*, 1–5, 2006.
14. Houze, R. A., "A climatological study of vertical transports by cumulus-scale convection," *J. Atmos. Sci.*, Vol. 30, 1112–1113, 1973.

15. Awaka, J., T. Iguchi, H. Kumagai, and K. Okamoto, "Rain type classification algorithm for TRMM precipitation radar," *Proceedings of the IEEE 1997 International Geosci. Remote Sen. Sym.*, 1636–1638, 1997.
16. Gamache, J. F. and R. A. Houze, "Mesocale air motions associated with tropical squall line," *Monthly Weather Review*, Vol. 110, 118–135, 1982.
17. Specifications of Distrometer RD-80, 2011, http://www.distromet.com/98.
18. Alonge, A. A. and T. J. Afullo, "Rainfall microstructures for microwave and millimeter wave link budget at tropical and subtropical sites," *2013 IEEE Africon Conference*, Le Meridien ile Maurice, Mauritius, Sep. 9th–12th, 2014.
19. Marshall, J. S. and W. M. Palmer, "The distribution of raindrops with size," *J. of Atmos. Sci.*, Vol. 5, 165–166, 1948.
20. Battan, L. J., *Radar Observations of the Atmosphere*, 323, University of Chicago Press, 1973.
21. Feingold, G. and Z. Levin, "The lognormal fit to raindrop spectra from frontal convective clouds in Israel," *J. Climate Appl. Meteor.*, Vol. 25, 1346–1363, 1986.
22. Ochou, A. D., A. Nzekou, and H. Sauvageot, "Parameterization of drop size distribution with rain rate," *Atmos. Res.*, Vol. 84, 5–66, 2007.
23. Sauvageot, H. and J. P. Lacaux, "The shape of averaged drop size distributions," *J. Atmos. Sci.,* Vol. 52, 1070–1083, 1995.
24. Nzekou, A., H. Sauvageot, A. D. Ochou, and C. M. F. Kebe, "Raindrop size distribution and radar parameters at Cape Verde," *J. Appl. Meteorol.*, Vol. 43, 90–105, 2004.
25. Houze, R., B. F. Smull, and P. Dodge, "Mesoscale organization of springtime rainstorms in Oklahoma," *Monthly Weather Review*, Vol. 118, 613–654, 1990.
26. Kozu, T. and K. Nakamura, "Rainfall parameter estimation from dual-radar measurements combining reflectivity profile and path-integrated attenuation," *J. of Atmos. and Oceanic Tech.*, 259–270, 1991.
27. Ulbrich, C. W., "Natural variations in the analytical form of the raindrop size distribution," *J. Climate Appl. Meteor.*, Vol. 22, 1764–1775, 1983.
28. Liebe, H. J., G. A. Hufford, and T. Manabe, "A model for the complex permittivity of water at frequencies below 1 THz," *Inter. J. of Infrared and Millimeter Waves*, Vol. 12, No. 7, 659–678, 1991.
29. Adetan, O. E. and T. J. Afullo, "Raindrop size distribution and rainfall attenuation modeling in equatorial subtropical Africa: Critical diameters," *Annals des Telecommunication*, 1–13, 10.1007/s12243-013-0418-z, 2014.
30. ITU-R Rec. P.838-3, "Specific attenuation model for rain for use in prediction methods," ITU-R, Geneva, 2005.
31. Ajayi, G. O. and R. L. Olsen, "Modeling of a tropical raindrop size distribution for microwave and millimeter wave application," *Radio Science*, Vol. 20, No. 2, 193–202, 1985.
32. Moumouni, S., M. Gosset, and E. Houngninou, "Main features of rain drop size distributions observed in Benin, West Africa, with optical disdrometers," *Geophysical Research Letters*, Vol. 35, L23807, 2008.
33. Maitra, A., "Rain attenuation modeling from measurements of rain drop size distribution in the Indian region," *IEEE Antennas Propag. Letters*, Vol. 3, 180–181, 2004.
34. Tokay, D. and A. Short, "Evidence from tropical raindrop spectra of the origin of rain from stratiform versus convective clouds," *J. Appl. Meteor.*, Vol. 35, No. 3, 355–371, 1996.
35. Short, D. A., T. Kozu, and K. Nakamura, "Rain rate and raindrop size distribution observations in Darwin," *Australia Proc. Open Symp. on Regional Factors in Predicting Radiowave Attenuation Due to Rain*, 35–40, URSI, 1990.
36. Stout, G. E. and E. A. Mueller, "Survey of relationships between rainfall rate and radar reflectivity in the measurement of precipitation," *J. of Appl. Meteor.*, Vol. 7, 165–174, 1968.
37. ITU-R Rec. P.837-6, "Characteristics of precipitation for propagation modelling," ITU-R, Geneva, 2012.